Iraqi J. Laser, issue 1, vol., 21, pp. 51-60 (2022)

IRAQI JOURNAL OF LASER

Mechanical Properties of AISI 316L Stainless Steel Produced Via Selective Laser Melting

Raid Mohammed Hadi[1], Ziad Aeyad Taha[2]

raed.mohammed1001a@ilps.uobaghdad.edu.iq *Corresponding author:*

[1, 2] *Institute of Laser for Postgraduate Studies, University of Baghdad*

(Received 21/04/2022; accepted 18/07/2022)

Abstract Additive manufacturing has been recently emerged as an adaptable production process that can fundamentally affect traditional manufacturing in the future. Due to its manufacturing strategy, selective laser melting (SLM) is suitable for complicated configurations**.** Investigating the potential effects of scanning speed and laser power on the porosity, corrosion resistance and hardness of AISI 316L stainless steel produced by SLM is the goal of this work. When compared to rolled stainless steel, the improvement is noticeable. To examine the microstructure of the samples, the optical microscopy (OM), scanning electron microscopy (SEM), and EDX have been utilized. Hardness and tensile strength were used to determine mechanical properties. The results indicated that the samples were completely dissolved, and the hardness was 285HV. Compared with the models produced by other parameters, the best 0.3% porosity was obtained using 100 W laser power, a hatching distance of 70 µm, a layer thickness of 30µm, and a scanning speed of 600 mm/sec. In addition, the volumetric energy density value for the best result was 79 J/mm^3.

Keywords: Additive Manufacturing, Stainless Steel SS316L, Selective Laser Melting, Volumetric Energy Density, Corrosion Resistance

1. Introduction

Lasers are nowadays used in various industries, such as welding, drilling, cleaning, and ablation [1-3]. Additive manufacturing (AM) is an impressive field for lasers in industrial applications, and it has a promising future. AM technology has lately attracted a lot of attention, mainly because of its high effectiveness in producing light-weight components and its recognized usefulness in fabricating parts with complicated interior characteristics [4-9]. Metal powder-based technologies are currently employed in the dentistry sector to manufacture tiny, durable, and corrosion-resistant prostheses [10]. The Selective Laser Melting (SLM) technology involves manufacturing a fully dense part in a layer-by-layer manner through the selective melting of a metallic powder bed [11]. Whereas this technology has the potential to open new directions for manufacturing machine parts; it has some flaws. The recognized faults include porosity, incomplete powder melting, insufficient dimensional and shape correctness, and significant surface roughness [12]. The rapid emergence of SLM as an emerging technology has aroused the industry sector's interest. One and the foremost reason behind this rapid popularity is the wide spectrum of applications that can AM technology aid in producing efficiently regardless of their complexity. aerospace, automotive, medicine, engineering and are typical examples of nowadays and promising applications. The austenitic stainless steel AISI 316L is noted for its superior corrosion resistance and mechanical qualities. Austenitic stainless steel has higher percentages of Cr and Ni in its composition than those existing in the ordinary steel. The Ni

presence improves corrosion resistance and stabilizes the austenite phase at low temperatures; 316L is protected from corrosion by a Cr_2O_3 oxide layer [13]. Because of its superior flexibility and corrosion resistance, austenitic stainless steel is one of the most often utilized alloys in the maritime, biomedical, and aerospace industries [14]. The aim of the present work is to study the effect of several SLM-related parameter including the power and scanning speed on key mechanical properties such as the porosity, corrosion resistance, wear resistance, and micro hardness of stainless steel 316L specimens, and then to calculate the VED for each set of parameters. In addition to comparing corrosion resistance with 316L samples made using the traditional approach.

2. Materials and methods

The SLM method uses the gas-atomized 316L stainless steel powder as the principal material for specimen fabrication. The powder has a nominal composition of Fe-17Cr-13Ni-2.5Mo-0.03C and a particle size of < 65µm. Cubic specimens (10×10×10 mm^3), as shown in Fig 1, were fabricated by the SLM technique. To avoid an oxidation phenomenon occurring during laser melting, this process was performed in an argon atmosphere using a 3D printer (M100) equipped with a continuous wave and a fiber laser of 300W. An approximate laser beam of 80 µm was used for the fabrication of specimens. The layer thickness for all the models was 30 µm. Rectangular samples of (60 × 12 × 2) mm, were manufactured for the uniaxial tensile test, which was machined according to ASTM E8 standard, as shown in Figure 2. Energy-dispersive X-ray spectrometry EDX was used for inspecting the proportions of the produced stainless steel sample's elements, as shown in Figure 3. And table 1 shows the percentage of elements of SS316L .Figure 4 shows the diagram of how the SLM process is performed inside the SLM100 machine. The 316L SS powders are delivered through a powder feeder, which uses a moving drum to create a powder bed; it is then totally melted by heat energy from a continuous or pulsed laser beam, and the steps are repeated layer by layer until the required shape is achieved. The temperature during the process was 80 C. The specimens were not heat-treated after being manufactured. The best volumetric energy density was calculated after stabilizing the power and changing the speed. The volumetric energy density is computed by equation 1.

$$VED = \frac{p}{vhd}\ J/mm^3 \quad ----- \quad (1)$$

Fig. 1: SLM as-manufactured specimens**.**

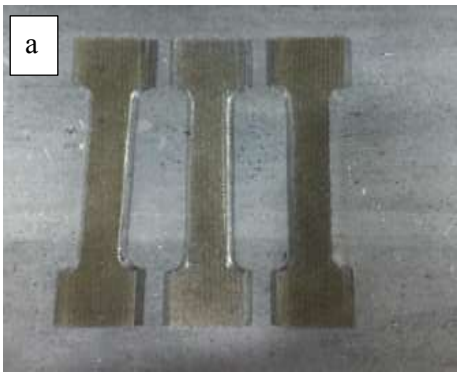

.

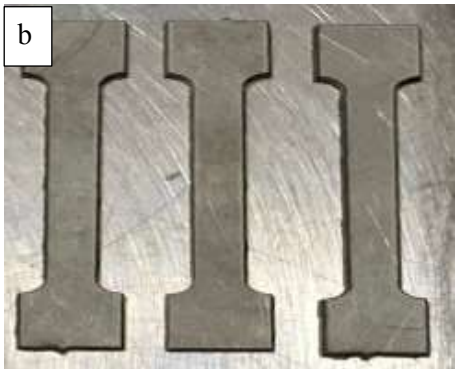

Fig. 2: **a**; SLM manufactured specimens **b**; conventionally manufactured, for tensile tests.

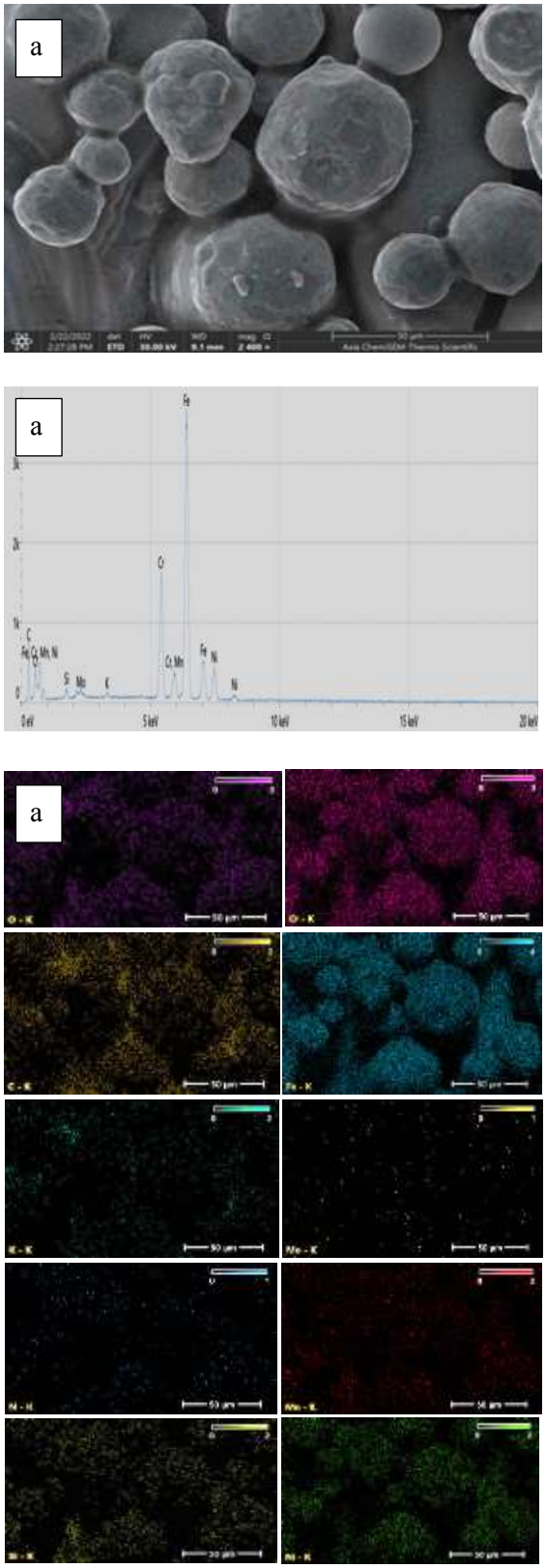

Fig. 3: EDX of AISI 316L by SLM. (a) SEM of the sample fabricated with a laser power of 100 W and scanning speed of 600 mm/s (b) EDX analysis performed on area marked. (c) EDX of individual elements maps

Where VED is the volumetric energy density of the powder bed (J/mm^3), P is the laser power (W), v is the laser scan speed (mm/s), h is the hatch distance (mm), and d is the powder bed layer thickness (mm) [15]. The corrosion test uses a Wenking MLab multichannel and SCI Mlab wear measurement system from Bank Electronics- Intelligent controls GmbH, Germany, as shown in Figure 5. A sliding wear resistance test was performed to investigate the coefficient of friction and the wear resistance of the AISI 316L, a steel ring was installed on the test machine, which was used for direct dry sliding contact with the testing surface of the sample, as shown in Figure 6.

Table (1) Shows the proportions of the ingredients of SS316L checked by EDS.

Weight % Error	Weight %	Atomic % Error	Atomic %	Element
0.6	17.4	1.5	42.8	C
0.5	2.4	1.0	5.1	N
0.5	6.8	0.9	12.6	O
0.0	1.0	0.0	1.0	Si
0.0	0.4	0.0	0.3	K
0.2	13.6	0.1	7.7	Cr
0.2	1.8	0.1	1.0	Mn
0.3	47.5	0.2	25.2	Fe
.2	7.6	0.1	3.8	Ni
0.9	1.6	0.3	0.5	Mo

Three groups have been made, each with a constant power at different speeds. The VED for each group was calculated by Equation No.1. The relationship between VED and porosity for each group after examining samples was then plotted to select the best criteria from each group. The relationship between VED and exact hardness was then determined to determine the best model among the pieces tested for wear and corrosion resistance. Figure 7 shows the relation between VED and porosity of each group. Figure 8 chooses the best sample from this set.

Table 2 summarizes the working procedures for this experiment.

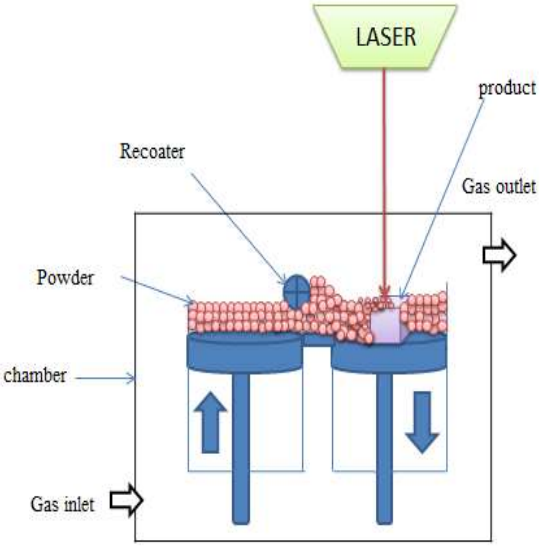

Fig. 4: schematic diagram that illustrates how the SLM process was conducted inside the machine.

Fig.5: Corrosion test

Fig. 6: wear test

Table (2) Experimental table of laser parameters.

Group	No	Power (W)	Scanning speed (mm/s)	VED ($J/mm^{3)}$
G1	S1	100	600	79
	S2	100	700	68
	S3	100	800	59
	S4	100	900	52
G2	S5	125	600	99.2
	S6	125	700	85
	S7	125	800	74.4
	S8	125	900	66
G3	S9	150	600	119
	S10	150	700	102
	S11	150	800	89
	S12	150	900	79

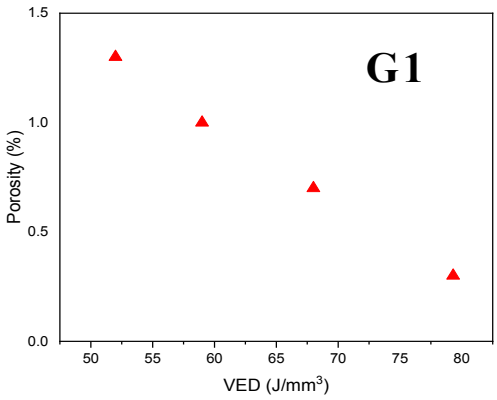

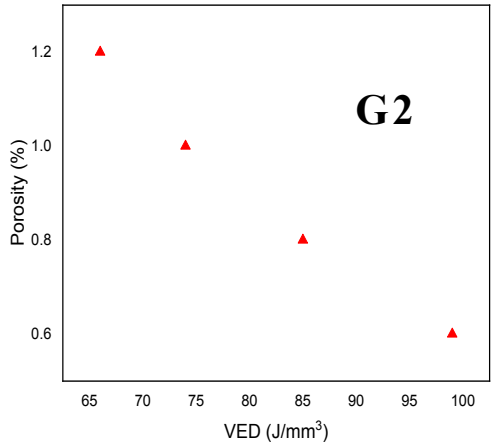

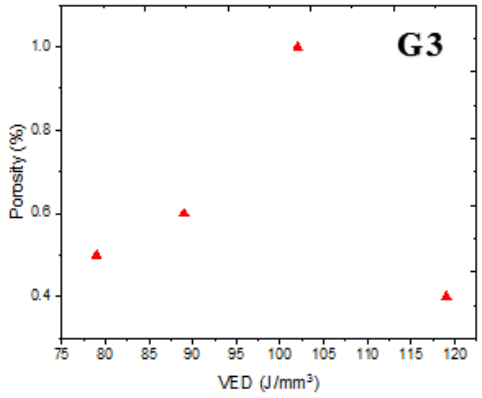

Fig.7: VED of samples produced with deferent porosity in G1, G2, G3**.**

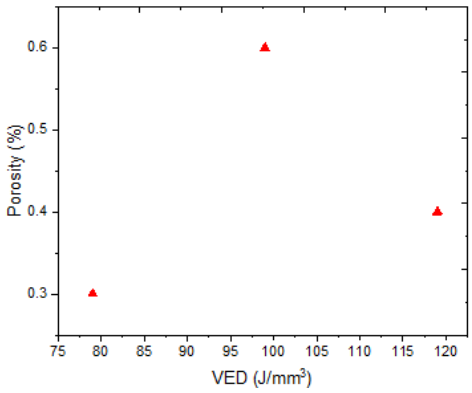

Fig. 8: The best graphic of the three groups to determine the best porosity and therefore the best parameters

3. Results and Discussion

The corrosion test results indicate that the SLM specimens are superior to the traditional samples. The mineral surface goes through three stages of behavior as shown in Fig 9. In addition, metal shows higher corrosion resistance and tends to be with uniform corrosion, where it is an inert layer with stable dynamic behavior. Pitting on the surface was apparent and very little, as in figure 10b, which means that the reaction with the solution occurs at a slow rate, and this means that the voltage continues as the inert layer continues. The potential increase to positive values (more noble alloy), meaning that the protection is higher[16] For the cast sample, the material began to interact due to interactions with the solution where it is clear from the beginning as in Figure 9. , The microstructure images in Figure 10a show that the surface corrosion of the poured sample is with clear and strong pitting, meaning that the protection range is very little. As a result of the interactions, where the layer stops creating and does not resist the oxidation reaction, and when the voltage rises, it generates bubbles that prevent the ions and electrons from interacting and therefore appear vertically. When it returns, it intersects the anodic curve at the point (0.328mA, 278mV), where it appears to have a limited scope for protection. Figure 11 depicts the SEM of the best sample at different magnifications as it reveals that some of the granules are bound to the body despite the completely dissolving powder. The remaining particle size of the adhesive powder and agglomerated particles appears at an additional magnification.

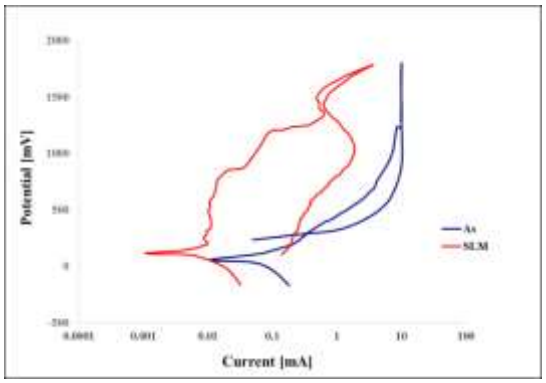

Fig. 9: Electrochemical characteristics of wrought stainless steel 316 L using, conventional method, SLM

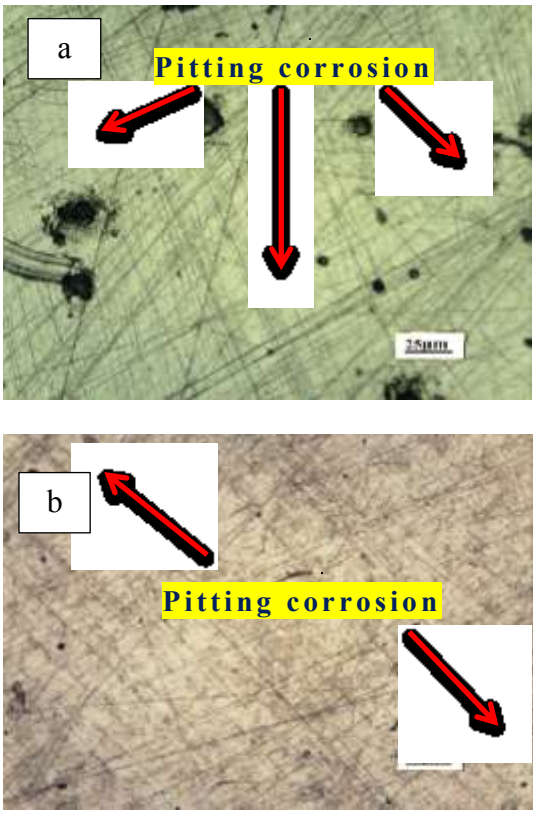

Fig. 10: Optical microscope of SS316L manufacturing by **a**; conventional method. **b**; SLM .

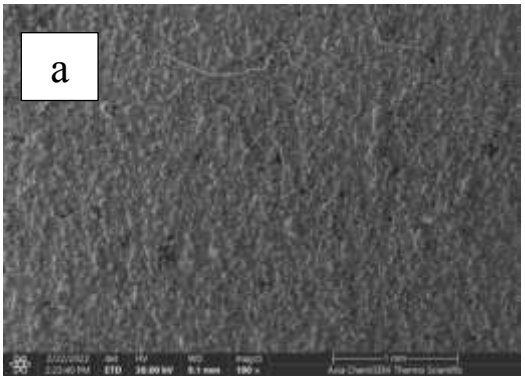

Fig. 11: SEM with magnification a; 100 X.

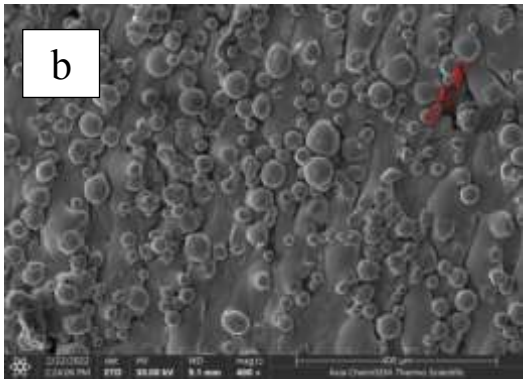

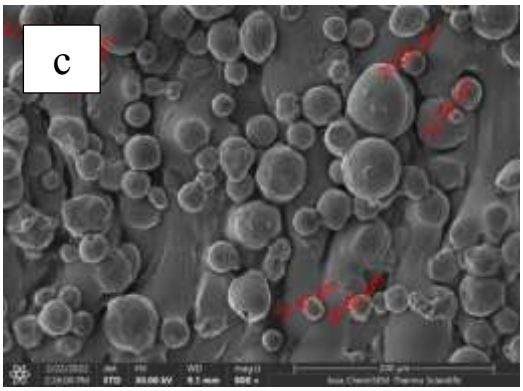

Fig. 11: SEM with magnification b; 400 X. c; 800X.

In the wear resistance test, the plowing process was evident in the rolled casting samples compared to the SLM-produced models; where the sliding type metal is clear and both pieces were subjected to the same load and period. The highest wear rate on the surface, and the difference gradually becomes less with increasing time. Wear is mainly through slippage of the load for the first time, and the microstructure is responsible for these properties. The product wear performance of SLM is better than that of rolled cast alloys, where the SLM samples were “ultra-hard” and more resistant to wear, with the time-frequency of the same load increases, as shown in Figure 12. A long period, the wear rate decreases due to the increase in deformation by removing parts of the sample surface after breaking the bumps. That is due to exposing the sample for a more extended period and thus more significant stress [17], as shown in Figure 13. The wear rate of

the SLM sample was 7.2E-9 (g/mm) while in rolled was 16E-9.

It was found that the difference in microhardness can be attributed to the scanning speed. Changes in the hardness value correspond to a certain scanning speed. Because the laser process has a fast cooling rate/cooling process, decreasing the scanning speed can lead to an increase in the heat accumulated in the material, which raises the temperature to the melting point and produces the molten phase. The highest hardness achieved was 285 HV for sample S1 of the first group, as shown in Figure 14, which has the highest density of 99.7% among the manufactured samples. These results of the high density that were obtained in the experimental are close to the literature by Bhowmik et al. [18], and Yusuf et al.[19].

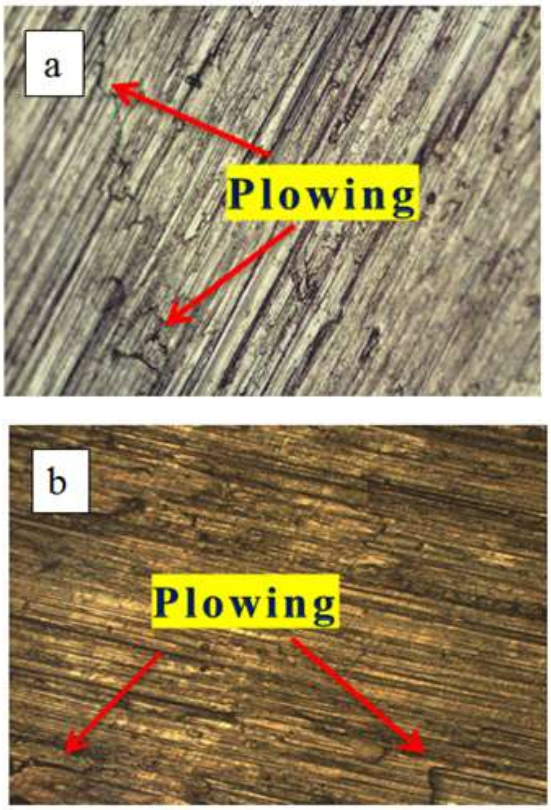

Fig. 12: Optical Microscope for Microstructure wear test for samples manufactured from SS316L **a)** Conventional method **b)** SLM.

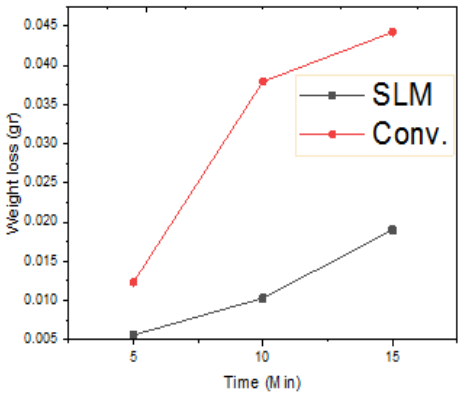

Fig.13: The difference in weight loss for rolled and SLM samples for the same load with a variable time.

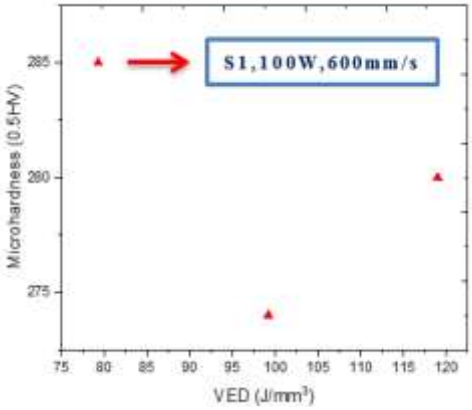

Fig.14: Micro hardness for samples with volumetric energy densitys.

In Figure 15, the samples were prepared and tested to measure the tensile strength at a junction velocity of 1 mm/min according to the ASTM-E8. According to Figure 16 (a), the rise in the load appears to reach 565MPa to break the SLM samples whereas it was 615MPa to break the rolled one. Figure 16 (b) reveals that while the high yield strength in the SLM case equals 480MPa and with low deformation of 9.8mm, the yield strength for rolled case was 260MPa and with high deformation of 27.9 mm. The intragranular cellular segregation network structure is confirmed to be the reason for improving the yield strength of the SLM SS316L compared with the SS316L fabricated by traditional methods [20].

Fig. 15: The tensile testing machine for tensile testing, samples after testing

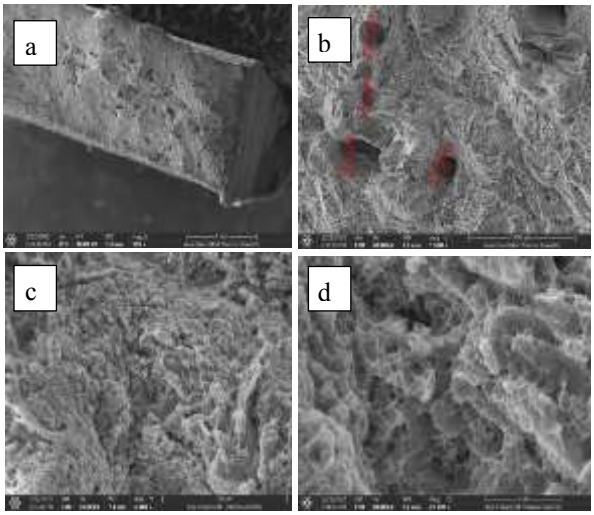

Fig. 17: Fractography for the SLM-316L sample after tensile strength. SEM images show (a) the fracture sample, (b) micro porosity, (c- d) completely melted regions.

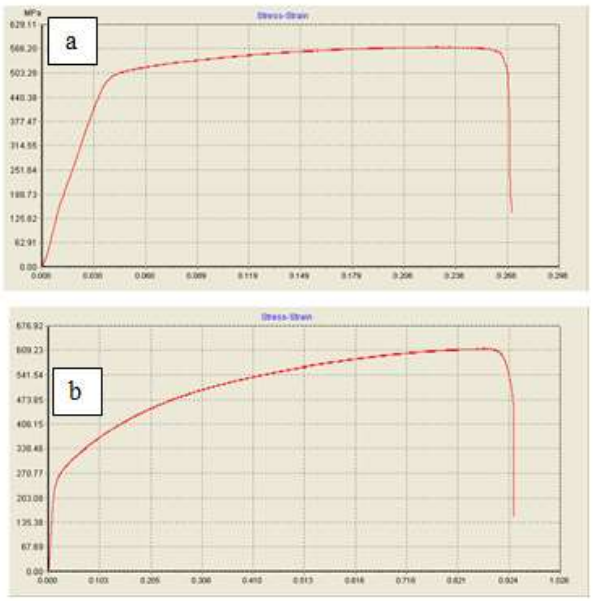

Fig. 16: Tensile strength for breaking sample a) 565MPa SLM b) 615MPa Conv.

The specimen fracture consists of uniformly distributed dimples. Most boils were larger than one micrometer and the dimples were uniform. More minor dimples indicate a lower deformation capacity. The micro pores in the sample of SLM can be noticed in Figure 17b.

Porosity is a common flaw in the SLM additive manufacturing and may adversely influence the mechanical characteristic. Gas-induced pores with nearly spherical shape occur during the gas deterioration of the 316L SS feedstock before the SLM process and may still present in the final product. [19]. The porosity lacks energy as it is insufficient to dissolve the powder completely. This leads to a lack of fusion or welding between each adjacent sweep and between successive layers. The excessive energy absorption leads to vaporization due to intense fusion, resulting in a keyhole. Fully molten areas are demonstrated in Figure 17(c) whereas Figure 17 (d) shows the boils.

4. Conclusions

The SLM316L proved a superior corrosion resistance over the as-cast counterpart due to a wider passive region, higher polarization resistance, and higher pitting potential. This was attributed to the lower density of micro-pores and the homogeneous distribution at the investigated scale. The SLM samples experience less plastic deformation than wrought samples. The wear resistance of the SLM parts is related to their high hardness and fine microstructure. The wear test reveals a highest and lowest wear due to the varying slip resistance under load. With increasing time, this distinction becomes less noticeable as the behavior in the SLM samples change. The results also show that the exact hardness of the samples ranges between 250 and 285 HV, and this was due to the different manufacturing parameters. This hardness was the highest compared to what was reported in the literature. The speed can play an important role in this criterion in the same manufacturing method. The analysis of the

image of the fractured sample after stretching under high magnification reveals that there is almost no porosity, indicating that the best sample of the selected groups is of the best parameter to achieve a high density of 99.7 percent.

References

[1] Z. A. Taha," Hole drilling of high density polyethylene using Nd: YAG pulsed laser", Iraqi Journal of Laser, vol. 18, no. 2, pp.41-46,2019.

[2] H. A. Jasim, G. A. Demir, B. Previtali, and A. Z. Taha, " Process development and monitoring in stripping of a highly transparent polymeric paint with ns-pulsed fiber laser," Optics & Laser Technology, vol. 93, pp. 60-66, 2017.

[3] A. F. Mutlak, M. Jaber, and H. Emad," Effect of Laser Pulse Energy on the Characteristics of Au Nanoparticles and Applications in medicine," Iraqi Journal of Science, PP. 2364-2369 , 2017.

[4]N. K. Rajak and Prof. A. Kaimkuriya, "Design and Development of Honeycomb Structure for Additive Manufacturing," International Journal of Trend in Scientific Research and Development, vol. Volume-2, no. Issue-6. South Asia Management Association, pp. 1198–1203, Oct. 31, 2018. doi: 10.31142/ijtsrd18856.

[5] R, Huang, et al, "Energy and emissions saving potential of additive manufacturing: the case of lightweight aircraft components," Journal of Cleaner Production, 135 PP.1559-1570. (2016).

[6]T. Xia et al., "Effect of Heat Treatment on Microstructure and Mechanical Properties of a Selective Laser Melting Processed Ni-Based Superalloy GTD222," Materials, vol. 14, no. 13. MDPI AG, p. 3668, Jun. 30, 2021. doi: 10.3390/ma14133668.

[7]L. E. Murr et al., "Fabrication of Metal and Alloy Components by Additive Manufacturing: Examples of 3D Materials Science," Journal of Materials Research and Technology, vol. 1, no. 1. Elsevier BV, pp. 42–54, Apr. 2012. doi: 10.1016/s2238-7854(12)70009-1.

[8]W. E. Frazier, "Metal Additive Manufacturing: A Review," Journal of Materials Engineering and Performance, vol. 23, no. 6. Springer Science and Business Media LLC, pp. 1917–1928, Apr. 08, 2014. doi: 10.1007/s11665-014-0958-z.

[9] N. T. Aboulkhair, N. M. Everitt, I. Ashcroft, and C. Tuck, "Reducing porosity in AlSi10Mg parts processed by selective laser melting," Additive Manufacturing, vol. 1–4. Elsevier BV, pp. 77–86, Oct. 2014. doi: 10.1016/j.addma.2014.08.001

[10]T. Kozior, J. Bochnia, P. Zmarzły, D. Gogolewski, and T. G. Mathia, "Waviness of Freeform Surface Characterizations from Austenitic Stainless Steel (316L) Manufactured by 3D Printing-Selective Laser Melting (SLM) Technology," Materials, vol. 13, no. 19. MDPI AG, p. 4372, Sep. 30, 2020. doi: 10.3390/ma13194372.

[11]Y. Huang et al., "Microstructure and wear properties of selective laser melting 316L," Materials Chemistry and Physics, vol. 254. Elsevier BV, p. 123487, Nov. 2020. doi: 10.1016/j.matchemphys.2020.123487

[12]A. Matras, "Research and Optimization of Surface Roughness in Milling of SLM Semi-Finished Parts Manufactured by Using the Different Laser Scanning Speed," Materials, vol. 13, no. 1. MDPI AG, p. 9, Dec. 18, 2019. doi: 10.3390/ma13010009.

[13]M. Mokhtari, P. Pommier, Y. Balcaen, and J. Alexis, "Laser Welding of AISI 316L Stainless Steel Produced by Additive Manufacturing or by Conventional Processes," Journal of Manufacturing and Materials Processing, vol. 5, no. 4. MDPI AG, p. 136, Dec. 14, 2021. doi: 10.3390/jmmp5040136.

[14]K. Chadha, Y. Tian, J. Spray, and C. Aranas, "Effect of Annealing Heat Treatment on the Microstructural Evolution and Mechanical Properties of Hot Isostatic Pressed 316L Stainless Steel Fabricated by Laser Powder Bed Fusion," Metals, vol. 10, no. 6. MDPI AG, p. 753, Jun. 05, 2020. doi: 10.3390/met10060753

[15]M. Letenneur, P. Imbrogno, A. Molavi Kakhki, and V. Brailovski, "Laser Powd Bed Fusion with Intentionally-Seeded Porosity for Prototyping of Powder Metallurgy Parts, " Journal of Manufacturing and Materials Processing, vol. 4, no. 4. MDPI AG, p. 119, Dec. 11, 2020. doi: 10.3390/jmmp4040119.

[16] X. Shang, Z. Wang, F. He, J. Wang, J. Li, and J. Yu, "The intrinsic mechanis of corrosion

resistance for FCC high entropy alloys," Science
China Technological Sciences, vol. 61, no. 2.
Springer Science and Business Media LLC, pp.
189–196, Oct. 17, 2017. doi: 10.1007/s11431
017-9114-1.
[17] Al-Khazraji, Mohammed Abdulateef Ahmed."Study Effect of Alternative Movement on rate of Dry and wet Wear and on The Microstructure of Structural Steel Type (A36ASTM)." DIYALA JOURNAL OF ENGINEERING SCIENCES 6.No.1, pp 24-36. (2013).
[18]A. Bhowmik, W. Zhai, W. Zhou, and S. M. L. Nai, "Characterization of carbide particle-reinforced 316L stainless steel fabricated by selective laser melting," Materials Characterization, vol. 179. Elsevier BV, p. 111360, Sep. 2021. doi: 10.1016/j.matchar.2021.111360.
[19]S. Yusuf, Y. Chen, R. Boardman, S. Yang, and N. Gao, "Investigation on Porosity and Microhardness of 316L Stainless Steel Fabricated by Selective Laser Melting," Metals, vol. 7, no. 2. MDPI AG, p. 64, Feb. 20, 2017. doi: 10.3390/met7020064.
[20]Y. Zhong, L. Liu, S. Wikman, D. Cui, and Z. Shen, "Intragranular cellular segregation network structure strengthening 316L stainless steel prepared by selective laser melting," Journal of Nuclear Materials, vol. 470. Elsevier BV, pp. 170–178, Mar. 2016. doi: 10.1016/j.jnucmat.2015.12.034.

الخواص الميكانيكية للفولاذ المقاوم للصدأ AISI 316L المُنتَج بواسطة الصهر الانتقائي بالليزر

رائد محمد هادي [1] زياد اياد طه [2]

[1، 2] معهد الليزر للدراسات العليا /جامعة بغداد

الخلاصة : لقد أثبت التصنيع الإضافي أنه عملية إنتاج قابلة للتكيف يمكنها تغيير التصنيع التقليدي بشكل أساسي في المستقبل. نظرًا لاستراتيجيتها التصنيعية ، فإن الصهر الانتقائي بالليزر (SLM) مناسب للتكوينات المعقدة. الهدف من هذا العمل هو التحقيق في تأثير سرعة المسح وقوة الليزر على المسامية ومقاومة التآكل والصلابة للفولاذ المقاوم للصدأ AISI 316L الذي تنتجه SLM. عند المقارنة بالفولاذ المقاوم للصدأ المدلفن ، فإن التحسن ملحوظ. لفحص البنية المجهرية للعينات ، استخدم الفحص المجهري البصري (OM) ، والمسح المجهري الإلكتروني (SEM) ، و EDX ،وكذلك قوة الشد والصلابة بالنسبة للخواص الميكانيكية . أوضحت النتائج أن العينات ذابت تماما وكانت الصلابة 285 HV. مقارنة بالنماذج التي تنتجها البراميترات الأخرى ، تم الحصول على أفضل مسامية 0.3٪ باستخدام طاقة ليزر 100 واط ، وفتحة مسافة 70 ميكرومتر ، وسمك طبقة 30 ميكرومتر ، وسرعة مسح 600 مم / ثانية. بالإضافة إلى ذلك ، كانت قيمة كثافة الطاقة الحجمية لأفضل النتائج 79 جول/ملم^3.